Pattern formation on the edge of chaos: Mathematical modeling of CO oxidation on a Pt(110) surface under global delayed feedback

Matthias Bertram and Alexander S. Mikhailov
Fritz-Haber-Institut der Max-Planck-Gesellschaft, Faradayweg 4-6, 14195 Berlin, Germany
(Received 11 December 2002; published 25 March 2003)

Effects of global delayed feedback on diffusion-induced turbulence are studied in a realistic model of catalytic oxidation of carbon monoxide on Pt(110). Spatiotemporal patterns resulting from numerical simulations of this model are identified and analyzed using a transformation into the phase and the amplitude of local oscillations. We find that chemical turbulence can be efficiently controlled by varying the feedback intensity and the delay time in the feedback loop. Near the transition from turbulence to uniform oscillations, various chaotic and regular spatiotemporal patterns—intermittent turbulence, two-phase clusters, cells of hexagonal symmetry, and phase turbulence—are found.

DOI: 10.1103/PhysRevE.67.036207 PACS number(s): 82.40.Bj, 82.40.Np, 05.45.Jn

I. INTRODUCTION

Self-organized pattern formation is a common feature of spatially extended nonlinear systems far from thermodynamic equilibrium [1]. In recent years, considerable progress was made in engineering pattern formation and controlling spatiotemporal chaos in such high-dimensional systems [2–6]. To achieve these goals, global control strategies are practical because in many distributed systems, where local access to all the individual elements is difficult, a single parameter that affects the dynamics of the entire medium can be easily manipulated.

By means of time-periodic external forcing, various patterns have been induced in oscillatory systems [7–9]. Wave propagation in excitable media can be controlled by the same method [10,11]. For practical applications, feedback methods are advantageous because an acting force is generated by the system itself, and thus the control signal automatically adjusts to variations of experimental conditions. Most feedback schemes designed for application to spatially extended systems aim to suppress spatiotemporal instabilities [12–14], but global feedbacks can also be employed as a tool to produce new spatiotemporal patterns [15]. Global feedbacks for controlling pattern formation under nonchaotic conditions were mainly applied to chemical systems [4,16–21], whereas the effects of such feedbacks on chaotic extended systems were also probed in systems of various other origins [3,22–25]. However, suppression of chemical turbulence was experimentally only recently achieved in the catalytic oxidation of carbon monoxide on a platinum(110) single crystal surface [5,26].

The experiments described in Refs. [5,26] employed a scheme of global delayed feedback that was proposed previously by theoretical investigations of a general model [15,27]. The feedback was implemented by making the CO partial pressure in the reaction chamber dependent on real-time properties of the evolving patterns. It was demonstrated that chemical turbulence can be controlled and replaced by various types of chaotic and regular spatiotemporal patterns.

In this paper, we study the effects of global delayed feedback on diffusion-induced turbulence in a realistic model of catalytic CO oxidation on Pt(110). The model approximately describes the experiments presented in Refs. [5,26]. The model reproduces experimentally observed phenomena and provides their theoretical interpretation.

The paper is organized as follows. The considered reaction, the model, and the feedback method are introduced in Sec. II. In Sec. III, the results of numerical simulations are presented. We show synchronization diagrams displaying the regions in parameter space where different types of spatiotemporal patterns exist. Those patterns are then analyzed by making use of a transformation to phase and amplitude variables that was introduced in Ref. [19] and is reviewed in the Appendix. The paper ends with a discussion of the obtained results in Sec. IV.

II. FORMULATION OF THE PROBLEM

Among oscillatory surface reactions, the catalytic CO oxidation on Pt(110) is the most thoroughly studied example [28]. Due to a high energy barrier in the gas phase, molecules of CO and oxygen have to adsorb on the catalytic surface before the reaction to carbon dioxide can take place (the adsorption of oxygen is dissociative). Produced CO_2 immediately desorbs into the gas phase leaving again free sites for adsorption of the reactants. The system is maintained far from thermodynamic equilibrium by a constant supply of fresh reactants and removal of the product.

The clean Pt(110) top surface layer reconstructs into a 1×2 ''missing row'' structure. This reconstruction can be reversibly lifted by adsorption of CO molecules [29]. Because oxygen adsorption is favored on the nonreconstructed 1×1 phase, periodic switching between two states of different catalytic activity can occur, resulting in temporal oscillations of the reaction rate.

Local spatial coupling across the catalytic surface is provided by surface diffusion of adsorbed CO molecules. Because the reaction consumes reactants from the gas phase and the resulting local variations of CO pressure in the gas phase quickly extend to the whole system, intrinsic global gas-phase coupling is always additionally present.

In the experiments described in Refs. [5,26], the effects of internal gas-phase coupling were minimized by using prefab-

TABLE I. Parameters of the model.

k_1	3.14×10^5 s^{-1} mbar^{-1}	Impingement rate of CO
k_2	10.21 s^{-1}	CO desorption rate
k_3	283.8 s^{-1}	Reaction rate
k_4	5.860×10^5 s^{-1} mbar^{-1}	Impingement rate of O_2
k_5	1.610 s^{-1}	Phase transition rate
s_{CO}	1.0	CO sticking coefficient
$s_{O,1\times1}$	0.6	Oxygen sticking coefficient on the 1×1 phase
$s_{O,1\times2}$	0.4	Oxygen sticking coefficient on the 1×2 phase
u_0, δu	0.35, 0.05	Parameters for the structural phase transition
D	40 μm^2 s^{-1}	CO diffusion coefficient
p_{O_2}	13.0×10^{-5} mbar	O_2 partial pressure
p_0	4.81×10^{-5} mbar	Base CO partial pressure
u_{ref}	0.3358	Reference CO coverage

ricated crystals with only small catalytically active areas. Pattern formation was monitored by means of photoemission electron microscopy (PEEM) [30]. The experimental parameters were chosen such that the reaction was oscillatory and, furthermore, uniform oscillations were unstable and a complex state of spiral-wave turbulence spontaneously developed. Global delayed feedback was artificially introduced by making the dosing rate of CO molecules dependent on the integral PEEM intensity in the observation window.

Mathematical modeling of the experiments is conducted using a realistic model of catalytic CO oxidation on Pt(110) [31,32]. The model takes into account adsorption of CO and oxygen molecules, reaction, desorption of CO molecules, the structural phase transition of the Pt(110) surface, and surface diffusion of adsorbed CO molecules. For simplicity, surface roughening, faceting, formation of subsurface oxygen, and the effects of internal gas-phase coupling are not taken into account. The equations are

$$\dot{u}=k_1 s_{CO} p_{CO}(1-u^3)-k_2 u-k_3 uv+D\nabla^2 u, \tag{1}$$

$$\dot{v}=k_4 p_{O_2}[s_{O,1\times1}w+s_{O,1\times2}(1-w)](1-u-v)^2-k_3 uv, \tag{2}$$

$$\dot{w}=k_5\left(\frac{1}{1+\exp\left(\frac{u_0-u}{\delta u}\right)}-w\right). \tag{3}$$

The variables u and v represent the surface coverage of CO and oxygen, respectively. The variable w denotes the local fraction of the surface area found in the nonreconstructed 1×1 structure. All three variables can vary in the interval from 0 to 1. For explanation and values of the parameters see Table I.

A variant of model (1)–(3) has first been studied in the absence of diffusion by Krischer *et al.* [31] and, after inclusion of diffusive coupling, by Bär *et al.* [33,34]. Depending on the values of its parameters, the model exhibits monostable, bistable, excitable, and oscillatory behaviors. The properties of stable rotating spiral waves and their breakup leading to turbulence were studied in quite detail in the excitable regime [34,35]. The existence of another form of chemical turbulence under oscillatory conditions was also subsequently shown [36]. Furthermore, the effects of internal gas-phase coupling and the influence of an additional variable accounting for the formation of subsurface oxygen have been investigated by Falcke and Engel [36–38] and by von Oertzen *et al.* [32] in different variants of the model.

To model the global delayed feedback applied in the experiments described in Refs. [5,26], we assume in this paper that the CO partial pressure p_{CO} in Eq. (1) is not constant but varies according to the equation

$$p_{CO}(t)=p_0-\mu[\overline{u}(t-\tau)-u_{ref}], \tag{4}$$

where $\overline{u}(t)=1/S\int_S u(\mathbf{x},t)\mathrm{d}\mathbf{x}$ denotes the spatial average of the CO coverage at time t. The parameter μ specifies the feedback intensity, τ is the effective time delay, and p_0 is the base value of partial CO pressure. The reference value u_{ref} is chosen as the CO coverage in the unstable steady state in the absence of feedback. The global feedback specified by Eq. (4) is designed in such a way that at vanishing delay, the CO partial pressure is instantaneously decreased when the integral CO coverage increases. The parameter τ allows to change the phase relation between an oscillating CO coverage and corresponding variations of the feedback signal. Note that in the experiments [5,26] the PEEM intensity, which is a nonlinear function of both the CO and oxygen coverages, was actually used to compute the control signal. However, the form of this function is not exactly known [30]. Thus, the description in Eq. (4) is a simplification of the experimental setup.

The effects of global delayed feedback on pattern formation in model (1)–(4) were previously investigated with parameter values chosen such that, in the absence of feedback, uniform oscillations were stable [19]. In contrast, in the present study the parameter values of the partial pressures are chosen such that uniform oscillations are unstable with respect to small perturbations and chemical turbulence spontaneously develops in the unperturbed system. As we shall see later, this leads to significant differences in the resulting phenomena when global feedback is applied.

Numerical simulations of the model were performed using a second-order finite difference scheme for the spatial discretization with a grid resolution of $\Delta x=4$ μm or smaller. For the temporal discretization an explicit Euler scheme with a fixed time step $\Delta t=0.001$ s is used. Long integration times of at least 3000s ensure that transients have decayed at the end of simulations. Unless stated otherwise, the system size is 0.8 mm for one-dimensional and 0.4×0.4 mm^2 for two-dimensional media, and periodic (no-flux) boundary conditions are imposed on one-dimensional (two-dimensional) systems. While for the two-dimensional system only selected frames of patterns are presented in this paper; short videos illustrating the evolution of different simulated two-dimensional patterns are available via Internet [39].

Spatiotemporal patterns resulting from numerical simulations of the model are identified and analyzed using a transformation of the model variables into the instantaneous phase and amplitude of local oscillations. To do this, we employ a method that was described in detail in Ref. [19] and is reviewed in the Appendix. Using this method, phase ϕ and amplitude R are defined in the projection plane of the two model variables u and w. A reference orbit for the dynamics defined in this plane is introduced to approximately compensate for deviations from harmonicity in the oscillations. A similar technique has been used also for the analysis of experimental patterns [26]. The transformation to phase and amplitude variables allows to directly compare the properties of patterns in systems of different origins. Moreover, it provides a link to general studies of pattern formation in oscillatory reaction-diffusion systems performed in the framework of the complex Ginzburg-Landau equation (CGLE) [40,41].

III. RESULTS

A. Amplitude turbulence

At first, the behavior found in model (1)–(4) in the absence of feedback ($\mu=0$) is considered. At the parameters specified in Table I, an isolated system element performs nonharmonic limit cycle oscillations of period $T_0=2.73$ s. However, due to destabilizing effect of the diffusive coupling between neighbored elements, uniform oscillations are unstable with respect to small perturbations and chemical turbulence spontaneously develops.

For a one-dimensional system, a space-time diagram showing the evolution of the variable u during transition from uniform oscillations to turbulence is displayed in Fig. 1(a). The initially small perturbations of the uniform state grow rapidly, thereby destroying spatial correlations between distant system elements. In the fully developed turbulent state, the spatially averaged values of all model variables are almost constant and show only small random fluctuations.

To further characterize the observed turbulent state, the transformation to phase and amplitude variables [19] is employed. Space-time diagrams of the phase and amplitude fields during the transition to turbulence are shown in Figs. 1(b) and 1(c), respectively. Here and in all further shown gray-scale images of the amplitude field, black color corresponds to $R=0$ and white color to the maximum value of R in the plotted distribution, unless stated otherwise. Examining Fig. 1(c), one finds that in the state of developed turbulence, multiple defects are present in the medium. Such objects are characterized by a significantly decreased oscillation amplitude. This state is reminiscent of *amplitude turbulence* [42] (or defect chaos [41]) in the complex Ginzburg-Landau equation.

At the same parameter values, uniform oscillations are also unstable in two-dimensional systems. Snapshots of the resulting spatial distributions of CO coverage, phase, and amplitude are displayed in Figs. 1(d), 1(e), and 1(f), respectively. The two-dimensional spatiotemporally chaotic state is characterized by the presence of extended regions of decreased oscillation amplitude (*strings*). Perpendicular to such objects, the oscillation phase strongly varies in space. The two ends of a string usually correspond to topological defects in the phase field. Fragments of spiral waves are only rarely visible in such a state of developed amplitude turbulence. The shown behavior represents a typical example of the turbulent state found in a wide range of model parameters.

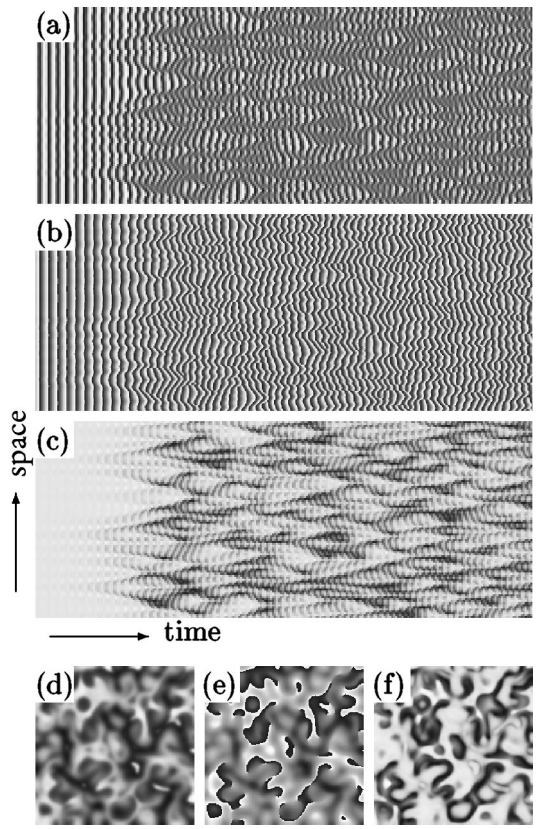

FIG. 1. Amplitude turbulence in model (1)–(4) in the absence of feedback ($\mu=0$). In frames (a), (b), and (c), space-time diagrams of CO coverage u, phase ϕ, and oscillation amplitude R, respectively, are shown for a one-dimensional system. The shown time interval is 150 s. Frames (d), (e), and (f) display snapshots of u, ϕ, and R, respectively, for a two-dimensional system. Darker regions in the images correspond to lower values of the displayed variables.

B. Overview of feedback effects

In the following study, we keep all parameters constant, except the feedback intensity μ and the delay τ, which are systematically varied. When global delayed feedback is present, it significantly affects the spatiotemporal self-organization of the system. The synchronization diagrams displayed in Fig. 2 summarize the results of multiple simulations of the one-dimensional system at different values of μ and τ. To uncover effects of hysteresis, the simulations underlying Fig. 2(a) started from the developed turbulent state, whereas Fig. 2(b) is based on simulations taking a uniform state with small superposed random perturbations as initial condition. Different types of stable regimes represented by different shading are reached after transients. Note that the two diagrams differ in the displayed range of feedback parameters.

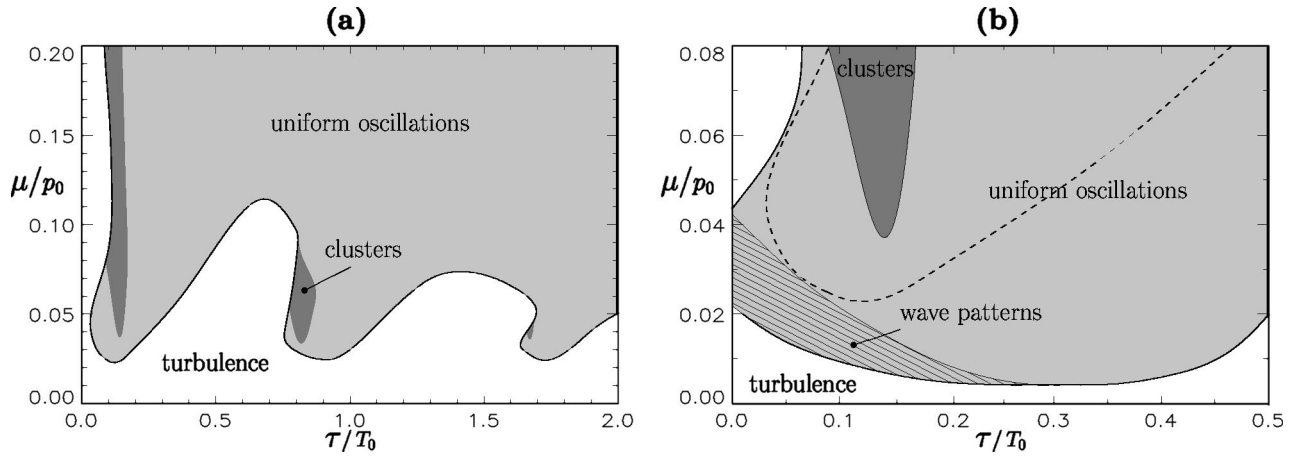

FIG. 2. Synchronization diagrams for the one-dimensional system in the presence of global delayed feedback, showing the approximate boundaries of different dynamical regimes reached after transients. The diagrams are based on numerical simulations that started with (a) developed turbulence and (b) a slightly perturbed uniform state as initial conditions. For comparison, the synchronization border in frame (a) is additionally shown in frame (b) as a dashed line. The delay time is measured in multiples of the oscillation period of the system in the absence of diffusion and feedback, $T_0=2.73$ s. The feedback intensity is normalized to the base CO partial pressure $p_0=4.81\times10^{-5}$ mbar. The shown boundaries have been determined from simulations with a density of sample points of $\Delta\mu/p_0=0.01$ and $\Delta\tau/T_0=0.01$ in the vicinity of the transition regions for frame (a) and with a density of $\Delta\mu/p_0=0.005$ and $\Delta\tau/T_0=0.01$ for frame (b).

Figure 2(a) shows that, if the feedback intensity is sufficiently large, global delayed feedback allows to suppress amplitude turbulence and induces uniform oscillations in a wide range of delays (light gray-shaded regions). The minimal value of μ needed to stabilize uniform oscillations, i.e., the efficiency of the feedback, strongly depends on the choice of τ. When the feedback intensity is fixed at an intermediate level, several synchronization windows alternate with turbulent zones upon variation of the delay. Note that in certain small intervals of the delay (e.g., in the approximate range $0.03<\tau/T_0<0.10$), turbulence can be suppressed at relatively low values of the feedback intensity, but the feedback fails to stabilize uniform oscillations at higher values of μ. At very small delays, $\tau/T_0<0.03$, the suppression of turbulence is impossible for realistic values of μ. The latter observation, however, is due to the specific implementation of global delayed feedback according to Eq. (4). Additional numerical simulations show that suppression of turbulence is also possible at arbitrarily small values of τ if, for instance, the generated control signal acts on the oxygen partial pressure p_{O_2} instead of on the CO partial pressure.

Even if global delayed feedback is too weak to completely suppress turbulence, it still can alter the properties of the turbulent state. An interesting dynamical regime is observed close to the synchronization border [the boundary between the white and the gray-shaded regions in Fig. 2(a)]. Here, a large part of the system is sometimes already in the state of uniform oscillations, but a few localized amplitude defects persist. Individual defects either die out in the further evolution of the system, or they initiate a cascade of defect reproduction. The resulting state is reminiscent of *intermittent turbulence* [42] (or spatiotemporal intermittency [41]) in the CGLE and is investigated more closely below.

At feedback parameters corresponding to the dark gray regions in Fig. 2, the turbulent state is suppressed via the formation of *cluster patterns*. Cluster patterns consist of large, homogeneously oscillating domains that are separated by narrow domain interfaces. As is shown later, two different types of stable clusters are observed: phase clusters with antiphase oscillations and amplitude clusters with coexistent limit cycles.

A different synchronization diagram is obtained when a uniform state with small superimposed random perturbations is taken as initial condition in the simulations, see Fig. 2(b). Examining this diagram, it is found that the stability region of uniform oscillations extends far beyond the former synchronization boundary [dashed line in Fig. 2(b)]. Thus, for a broad range of delays, the uniform state shows strong hysteresis when the feedback intensity is decreased from large values. Turbulence spontaneously develops from almost uniform initial conditions only at feedback parameters outside the shaded regions. However, in the intermediate parameter range inside the shaded regions but below or to the left of the dashed line, a sufficiently strong local perturbation of the uniform state is able to initiate a defect cascade, yielding either intermittent or fully developed turbulence. The formation of clusters is not noticeably affected by hysteresis effects.

Further types of patterns exist in the hatched region in Fig. 2(b). In this region, uniform oscillations are unstable, and *wave patterns* characterized by an intrinsic wavelength develop from small random perturbations. The parameter region where wave patterns develop in the one-dimensional system approximately coincides with the parameter range for which *cellular structures* are found in the two-dimensional system. Wave patterns, cellular structures, and their transition to turbulence are also further discussed in the following sections.

C. Intermittent turbulence

Intermittent turbulence is characterized by the occurrence of turbulent bursts on a laminar background. In this regime,

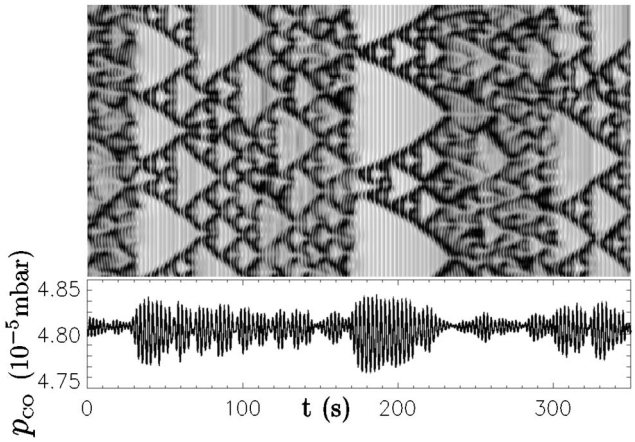

FIG. 3. Space-time diagram of intermittent turbulence in a one-dimensional system. The amplitude R is plotted; dark color denotes low amplitude values. Below the space-time diagram, the corresponding chaotic temporal variations of the CO partial pressure are shown. The feedback parameters are $\tau/T_0=0.293$ and $\mu/p_0=0.043$.

a certain degree of long-range order is retained. An example of such behavior is displayed in Fig. 3. The chosen parameter values are close to the synchronization border in Fig. 2(a). The resulting state is characterized by repeated cascades of amplitude defects on the background of uniform oscillations. The defects reproduce until nearly the entire system is covered with turbulence. Then, they simultaneously annihilate in some parts of the medium. Sometimes only a few defects survive and initiate another reproduction cascade. In this way, the system behavior alternates between strongly turbulent states with only short-range spatial correlations and nearly uniform states with large-scale spatial correlations. Note that the global oscillations used to generate the feedback signal in the state of intermittent turbulence are chaotic.

The transition from fully developed to intermittent turbulence and to uniform oscillations in our model is as follows. When the feedback is introduced, small areas with uniform oscillations appear. As the feedback intensity is increased, the number of such areas and their average size grow. At a critical value of μ, all defects die out after transients and the oscillations are uniform. This corresponds to the crossing of the synchronization border in Fig. 2(a) from below. In small systems, the delay-dependent transition point depends on the system size and the critical value of μ is lower for smaller systems. This dependence saturates for larger systems of size $L\approx 1$ mm. Intermittent turbulence is also observed as a transient above the synchronization border in Fig. 2(a); however, in this case, all defects finally die out. As the feedback intensity is decreased from large values towards the synchronization border, the lifetime of defects rapidly increases.

In two space dimensions, intermittent turbulence is characterized by irregular cascades of nearly circular structures on the background of uniform oscillations. Figure 4 displays three subsequent snapshots of the spatial distributions of CO coverage, phase, and amplitude in such a pattern. Additionally, phase portraits are shown in the bottom row of Fig. 4,

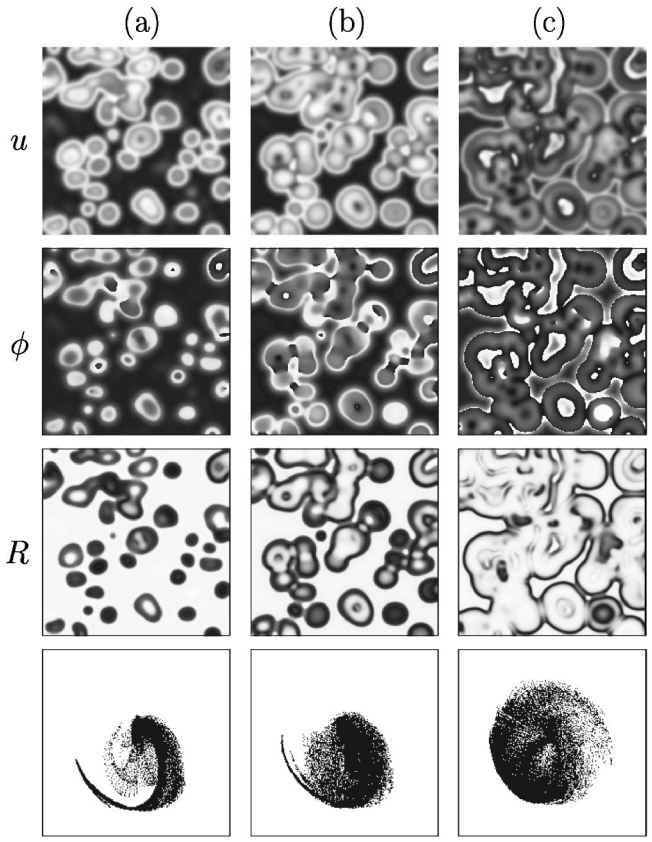

FIG. 4. Snapshots of CO coverage (top row), phase (second row), amplitude (third row), and phase portraits (bottom row) for intermittent turbulence in two space dimensions. The time interval between the subsequent images shown in each row is $\Delta t=5.2$ s and approximately corresponds to two periods of the oscillating background. The system size is 0.6×0.6 mm^2. The parameter values are $\tau/T_0=0.293$ and $\mu/p_0=0.056$. A short video illustrating the evolution of bubbles and ring-shaped structures during intermittent turbulence is available via Internet [39].

obtained by plotting the amplitudes and phases for all pixels of a pattern in polar coordinates. The phase of a point in the phase portrait is represented by the polar angle and the amplitude by the distance to the coordinate origin.

At constant feedback parameters, the pattern evolution is as follows: at a given instant, individual bubbles and ring-shaped structures are present on an almost uniform background, see Fig. 4(a). The ring-shaped structures represent a later stage in the evolution of bubbles. They are similar to the strings observed during fully developed turbulence, but their shape typically is more circular. Inside the localized bubbles and along the border of the ring-shaped objects, the oscillation amplitude is strongly decreased. The phase varies strongly in space perpendicular to such objects. A distinct structure is then found in the phase portrait shown in the bottom of Fig. 4(a), where the uniform background corresponds to the sharp end of the tail. As time goes on, the localized bubbles grow in size and transform into expanding rings, see Fig. 4(b). New turbulent bubbles are then created inside such structures. During this process, the structure in the phase portrait slowly scatters. When the expanding rings

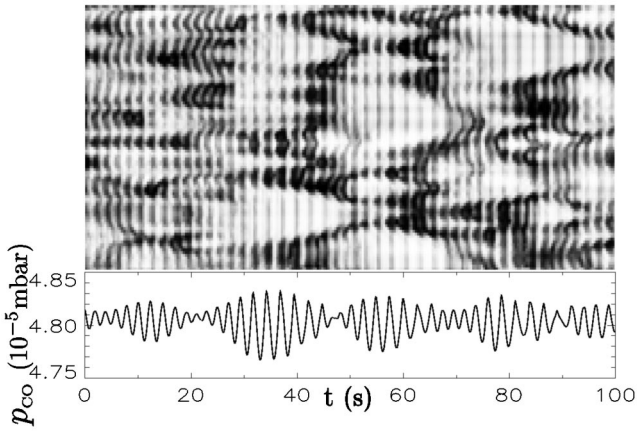

FIG. 5. Pattern evolution along a cross section through a two-dimensional pattern representing intermittent turbulence. A space-time diagram of the amplitude distribution and the variation of CO partial pressure are displayed. The same parameters as in Fig. 4.

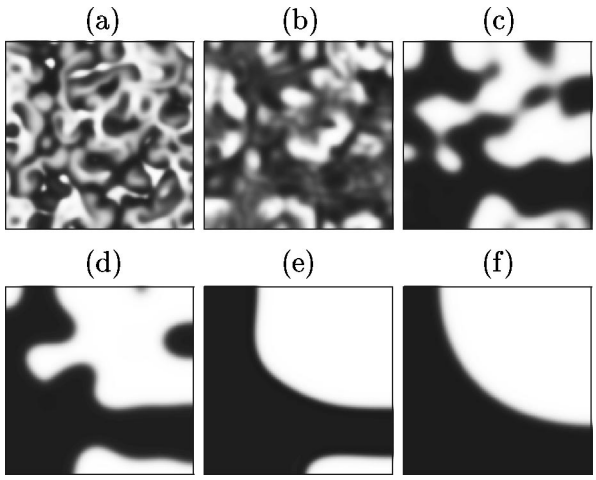

FIG. 6. Development of phase clusters from amplitude turbulence in two space dimensions. The variable u is displayed at different points in time after global feedback has been switched on: (a) $t=0$ s, (b) $t=8.2$ s, (c) $t=16.4$ s, (d) $t=28.6$ s, (e) $t=98.2$ s, and (f) $t=294.5$ s. The parameter values are $\tau/T_0=0.147$ and $\mu/p_0=0.083$.

gain direct contact, they merge, such that a few oscillation periods later, only small laminar regions are left in the system, as displayed in Fig. 4(c). In this state, extended line defects with almost vanishing amplitude separate the remaining uniform regions from parts of the medium now covered by turbulence. Another such evolution cycle is again initiated some time later, after large parts of the turbulent regions have again spontaneously synchronized and only a few localized defects have survived.

The pattern evolution along a cross section through the two-dimensional system is shown in Fig. 5. It is characterized by irregular reproduction cascades of defects similar to the one-dimensional case. However, the two-dimensional case is more complicated since localized objects expanding into the cross section may emerge spontaneously in the space-time diagram. Note that the temporal oscillations of R in the space-time diagram are an artifact of the approximate transformation to amplitude and phase variables due to strong deviations of the local dynamics from the chosen reference orbit in phase space.

The observed properties of intermittent turbulence agree well with the scenario seen in the CGLE with global feedback. In this equation, remarkably similar cascades of amplitude defects have been observed in one space dimension [15,43]. In two dimensions, the defects corresponded to bubble-shaped structures [27]. Note that intermittent turbulence has also been observed in the unforced CGLE for appropriate parameter values [41,44]. However, it looks different and ring-shaped objects are usually not observed in this case in two space dimensions.

D. Cluster patterns

Inside the cluster regions in Fig. 2, two different types of stable clusters, the so-called phase and amplitude clusters, have been observed. Their common feature is the presence of a small number of synchronized domains belonging to one of two different oscillatory states. No intrinsic spatial wavelength is present in such patterns.

For most choices of the feedback parameters inside the cluster regions in Fig. 2, two-phase clusters develop. Starting from amplitude turbulence, consecutive snapshots during the development of such a pattern are displayed in Fig. 6. On the time scale of a few seconds, amplitude turbulence is gradually suppressed and synchronized domains with antiphase oscillations develop [Figs. 6(a)–6(c)]. The initial spatial distribution of such domains is random. During the further evolution, individual cluster domains of the same phase merge and smaller domains die out [Fig. 6(c)–6(e)]. A further slow drift of the phase fronts is then still observed, with a tendency to minimize the front curvature. Finally, a stable stationary distribution is reached [Fig. 6(f)].

An important property of phase clusters in our model is phase balance, i.e., the total areas occupied by the different phase domains in the asymptotic state are equal. When a simulation is started with a different initial size ratio, the domain interfaces slowly drift until a balanced configuration is reached. This drift is induced by the change in the feedback signal that follows a change of the size ratio. In the state of phase balance, the local oscillations sum up to a global signal with a frequency twice as large as the frequency of local oscillations, see the curves below the space-time diagram of one-dimensional phase clusters displayed in Fig. 7. Two-phase clusters with similar properties were also found in our previous investigations [19] of feedback-induced pattern formation when uniform oscillations were stable and turbulence was absent in the unperturbed system.

The space-time diagram in Fig. 7 reveals an interesting difference from the previously observed phase clusters. Examining this diagram, one finds that the local oscillations inside the phase domains are characterized by an alternating magnitude of subsequent oscillation maxima (see also the curves below the space-time diagram). This phenomenon of period-two oscillations significantly affects the properties of the narrow phase fronts separating the different domains.

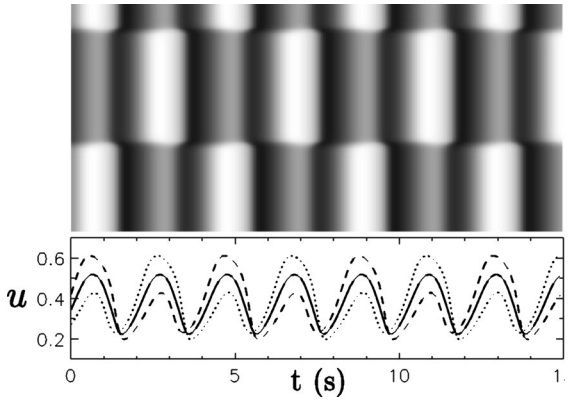

FIG. 7. Space-time diagram of phase clusters in a one-dimensional system. The variable u is displayed. The curves in the bottom show the variation of CO coverage u within the different cluster domains (dashed and dotted lines) and the variation of the spatial average $\bar{u}$ (solid line). The same parameters as in Fig. 6.

While within the domains, consecutive local oscillation maxima show a large difference, this difference continuously decreases towards the center of a phase front. In the middle of the front, there is a point where the oscillations are of period-one type and almost coincide with the global oscillations of the pattern (black line in Fig. 7). Thus, an oscillation node is absent inside such stationary fronts. This result contrasts with the presence of oscillation nodes typical for stationary antiphase domains with period-one local oscillations [19,45].

Additionally, a different cluster type exists in the large cluster region in Fig. 2(a) (at $\tau/T_0 \approx 0.15$) at high feedback intensities, $\mu/p_0 > 0.17$. A space-time diagram of such clusters, which are due to the coexistence of two limit cycles, is shown in Fig. 8. Inside the small domain, oscillations are simple periodic and have a large amplitude, while the other domains of the pattern show period-two oscillations with much smaller amplitude. The domain interfaces are stationary and phase balance is absent in such a pattern. Clusters

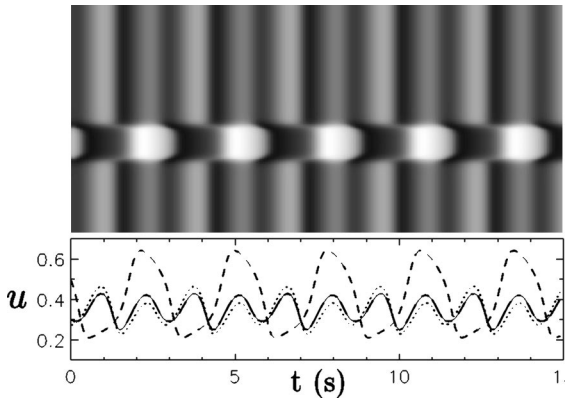

FIG. 8. Space-time diagram of clusters with coexisting limit cycles in a one-dimensional system. The variable u is displayed. The curves show the variations of u within the small and the large cluster domains (dashed and dotted lines, respectively) and the variation of $\bar{u}$ (solid line). The parameter values are $\tau/T_0 = 0.088$ and $\mu/p_0 = 0.200$.

with coexisting limit cycles (''amplitude clusters'') were also observed in the model of CO oxidation as an effect of global delayed feedback on stable uniform oscillations [19] and under intrinsic gas-phase coupling [36,37].

E. Wave patterns and cellular structures

In the following, patterns found in the hatched region in Fig. 2(b) are described. All such structures are stable with respect to small perturbations, but transform into intermittent or developed turbulence when a sufficiently strong local perturbation is applied.

Close to the upper boundary of this region, oscillatory *standing waves* with an intrinsic wavelength are found in one space dimension, see Fig. 9 for an example. Such patterns consist of periodic modulations of both the spatial distributions of the oscillation phase and the amplitude, see Fig. 9(a). A local increase of R corresponds to a decrease of ϕ. The modulations are stationary, so that all system elements show periodic oscillations, see the space-time diagram of the oscillation phase shown in Fig. 9(b). The phase and amplitude variations are small for feedback parameters close to the border to uniform oscillations, and continuously grow as the feedback intensity is decreased at a constant delay. At a given set of feedback parameters, the wavelength of the modulations is a characteristic property of the pattern, i.e., it is almost independent of the system size (a weak dependence is still observed due to the constrains set by the periodic boundary conditions). Standing waves arising from a finite wavelength instability were previously observed in the model of CO oxidation under intrinsic gas phase coupling [36,37] and in the CGLE with global feedback [15].

Upon a decrease of the feedback intensity, standing waves become unstable when the amplitude and phase modulations have reached a critical size. Neighboring phase minima then start to oscillate weakly around their mean position, thereby forming a pattern of *breathing waves*. A space-time diagram showing the phase distribution of such a pattern in a rotating coordinate frame is shown in Fig. 10(a). When μ is further decreased and the strength of the breathing reaches the order of the spatial wavelength of the pattern, its regularity breaks down. The resulting state is shown in Fig. 10(b). Colliding local phase minima merge and from time to time new such regions are created. However, the phase and amplitude modulations remain comparatively weak, and the global oscillations are still nearly periodic. Such a behavior is reminiscent of *phase turbulence* [41] in the one-dimensional CGLE. Defects are only spontaneously created in the system when the feedback intensity is further decreased below the hatched region in Fig. 2(b), where they quickly reproduce to form amplitude turbulence. The described transition from standing waves to breathing waves and to phase turbulence is in accordance with previous observations in the framework of the CGLE with global feedback [43].

In roughly the same region of feedback parameters where wave patterns and phase turbulence are found in one space dimension, oscillatory cellular structures develop in two-dimensional systems. Like wave patterns, such structures represent small-amplitude modulations of uniform oscilla-

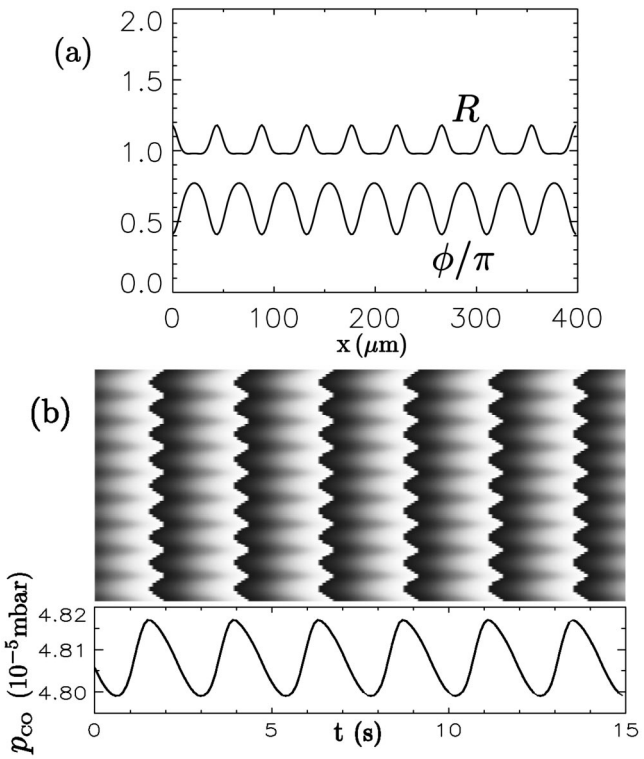

FIG. 9. Standing waves in a one-dimensional system. (a) Phase and amplitude profiles at a fixed time. (b) Space-time diagram of the phase and the corresponding variation of the CO partial pressure. The parameter values are $\tau/T_0=0.110$ and $\mu/p_0=0.012$.

tions and are replaced by intermittent or amplitude turbulence upon a sufficiently large local perturbation. Three different types of cellular structures are encountered. Close to the border to uniform oscillations, the cell arrays are regular and show a hexagonal symmetry, see Fig. 11(a). Such patterns are the result of nonlinear interactions between triplets of modes of wave vector $\mathbf{k}$ with the same wave number $|\mathbf{k}|=k_0$ [46]. The observed structures are stationary in space, but show time-periodic local oscillations.

When the feedback intensity is decreased, stationary cell arrays become unstable at a delay-dependent critical value of μ. Individual cells then periodically shrink and expand, thereby forming an array of breathing cells, see Fig. 11(b). In the spatial Fourier spectrum of such a pattern, two independent frequencies are present.

As in the one-dimensional system, phase turbulence develops upon further decrease of the feedback intensity. A snapshot of the resulting state, characterized by the mobility of cells, is shown in Fig. 11(c). Individual cells shrink and expand aperiodically while they slowly travel through the medium. Occasionally, some of the cells die out or, following an expansion, reproduce through cell splitting, see Fig. 12 for such an event. Phase turbulence is replaced by amplitude turbulence when the feedback intensity is further decreased. The formation of oscillatory cellular structures was also theoretically studied in the general model of the CGLE with global feedback [27,46].

IV. DISCUSSION

In this paper, we have shown that amplitude turbulence in a realistic model of CO oxidation on Pt(110) can be suppressed by means of global delayed feedback. Such a feedback can be easily implemented in systems of various origins and its parameters can be freely varied. Synchronization diagrams have been constructed for different initial conditions, showing the regions of existence for different spatiotemporal patterns. It was found that turbulence is suppressed and uniform oscillations are stabilized in wide regions of the feedback parameters, in accordance with experimental findings [26]. At the edge of chaos, when global delayed feedback is too weak to induce uniform oscillations but strong enough to significantly affect pattern formation, a broad variety of complex patterns was found.

In Fig. 13, we summarize the different observed two-dimensional structures and their amplitude and phase properties. The images in the top, second, and third rows of Fig. 13 display spatial distributions of CO coverage, phase, and amplitude, respectively. Additionally, the bottom row shows a phase portrait of each pattern.

The unperturbed turbulent state [Fig. 13(a)] is characterized by strong amplitude and phase fluctuations. This state is similar to fully developed amplitude turbulence in the unforced CGLE [41]. The patterns shown in Figs. 13(b)–13(e) represent typical two-dimensional patterns induced by the feedback.

Intermittent turbulence [Fig. 13(b)] has been observed close to the synchronization border under increasing feedback intensity. This regime is characterized by irregular cascades of bubbles developing into ring-shaped structures on the background of uniform oscillations. The amplitude is strongly decreased inside such localized objects.

Stationary two-phase clusters [Fig. 13(c)] were observed under further increase of the feedback intensity in narrow intervals of the delay time τ. Because the local oscillations inside the cluster domains exhibit period-two local oscillations, oscillations within the different cluster domains at a given point in time differ not only in phase, but also in amplitude; nonetheless, they correspond to the same limit cycle. In addition to phase clusters, amplitude clusters with coexistent limit cycles were also observed but are not shown in Fig. 13.

Hexagonal cell arrays [Fig. 13(d)] arising from a finite wavelength instability were found in a range of feedback parameters where standing waves develop in one space dimension. Secondary instabilities led to breathing cellular structures (not shown in Fig. 13), and to phase turbulence [Fig. 13(e)]. As seen in the corresponding phase portraits, both the phase and the amplitude are modulated in cellular structures, though the amplitude variations are weak.

All principal types of feedback-induced two-dimensional patterns—intermittent turbulence, clusters, and cellular structures—were also observed in experiments with CO oxidation on Pt(110) under global delayed feedback [5,26]. During intermittent turbulence, not only the formation of bubble-shaped objects on a uniformly oscillating background was experimentally observed, but also their predicted reproduc-

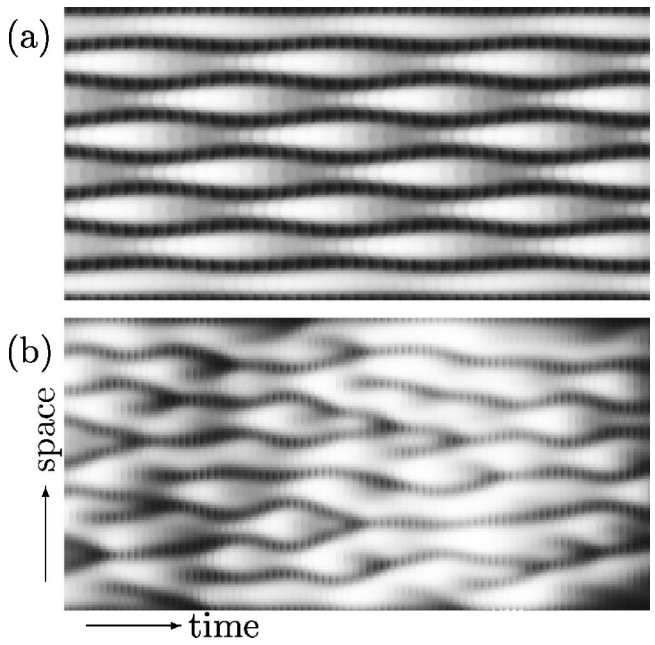

FIG. 10. Space-time diagrams of (a) breathing waves and (b) phase turbulence in a one-dimensional system. The phase distribution is displayed in a coordinate frame rotating with the period of the reference orbit. The shown time intervals are (a) 100 s and (b) 200 s. The parameter values of τ/T_0 and μ/p_0 are, respectively, (a) 0.110, 0.010, and (b) 0.110, 0.008.

tion cascades could be identified. Phase clusters in the experiments also exhibited stationary phase fronts, period-two local oscillations, and phase balance. While disordered cellular structures have been observed, regular arrays of cells were not seen in the experimental system where finetuning of the parameters is difficult and some structural surface defects are always present. Additionally, the experiments exhibited a variant of standing waves characterized by the presence of alternating dark and bright stripes. It is known that in order to reproduce such patterns in simulations employing the model of CO oxidation, a fourth variable describing the formation of subsurface oxygen must be included [32].

A transformation to phase and amplitude variables similar to the one we have employed in the present work has also been applied to the experimental data [26]. Our simulations successfully reproduce the principal amplitude and phase properties of the corresponding structures seen in the experiments. There, the turbulent objects seen during intermittent turbulence also represent extended amplitude defects. For two-phase clusters, a similar ''bridge'' connecting the two different phase states is seen in the phase portraits. Cellular structures in the experiments are also characterized by relatively strong phase variations while the amplitude variations are comparatively weak.

The results of our simulations can be further compared to the previous study [19] of model (1)–(4) conducted at parameter values for which the unforced system shows stable uniform oscillations (or stable spiral waves in two space dimensions) instead of chemical turbulence. For this case, a different synchronization diagram featuring spatiotemporal

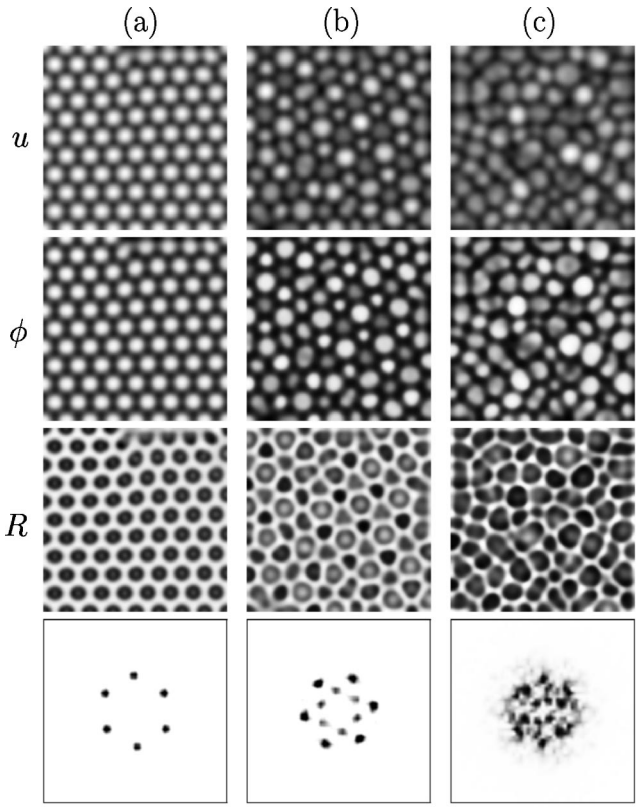

FIG. 11. Different types of oscillatory cellular structures in two space dimensions: (a) stationary cells, (b) breathing cells, (c) phase turbulence. Displayed are distributions of CO coverage (top row), phase (second row), amplitude (third row), and the spatial power spectra of the amplitude distributions (bottom row). In the images of u, ϕ, and R, black color corresponds to the minimum and white color to the maximum value of displayed variables. The parameter values of τ/T_0 and μ/p_0 are, respectively, (a) 0.110, 0.019; (b) 0.110, 0.016; and (c) 0.110, 0.012.

patterns such as traveling phase flips, asynchronous oscillations, and several other types of cluster patterns was obtained. Except for clusters, none of the structures presented in the present study were observed. Bubbles and ring-shaped structures during intermittent turbulence, oscillatory cellular structures, and phase turbulence are characteristic patterns near a transition to chaos and thus we conclude that the pres-

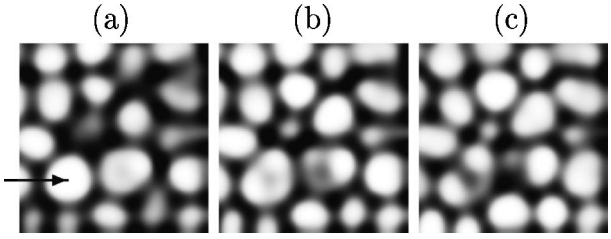

FIG. 12. Splitting process of a cell. The cell that undergoes splitting is indicated by an arrow. Snapshots of the phase are displayed; only one quarter of the system of size 0.4×0.4 mm^2 is shown. The time interval between individual frames is $\Delta t=4.8$ s. The parameters are as in Fig. 11(c).

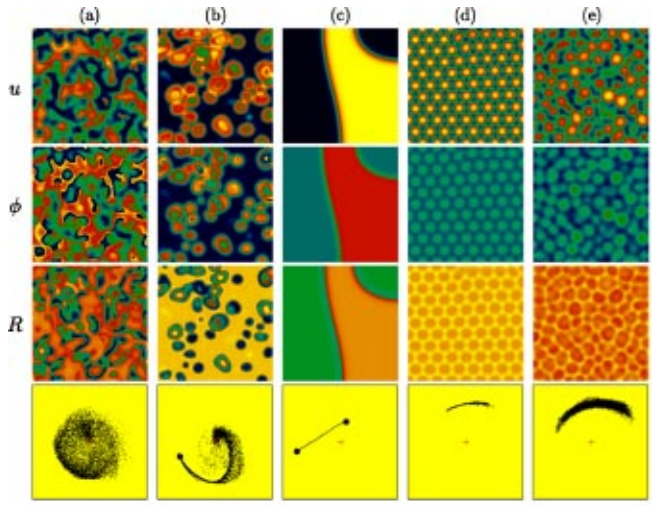

FIG. 13. (Color online) Distributions of CO coverage (top row), oscillation phase (second row), amplitude (third row), and phase portraits (bottom row) for (a) unforced turbulence and (b)–(e) several typical feedback-induced two-dimensional patterns. In the images, yellow (white) color denotes high, and blue (black) color denotes low values of the displayed variables. Green and red (light and dark gray, respectively) areas denote intermediate values. The phase portraits display amplitude and phase of each pixel of a pattern in polar coordinates. In the phase portraits (b) and (c), bold dots have been added to indicate the uniform states. The side length of the system is 0.4 mm in frames (a), (c)–(e) and 0.6 mm in frame (b). The values of the feedback parameters μ (10^{-5} mbar) and τ (s) are, respectively: (a) 0, 0; (b) 0.27, 0.8; (c) 0.40, 0.4; (d) 0.09, 0.3; and (e) 0.06, 0.3.

ence of turbulence in the unforced system is essential for their observation.

We finally note that in our numerical study, the model parameters have been chosen in such a way that oscillations were not harmonic and the system was not close to a supercritical Hopf bifurcation. Nonetheless, the observed patterns, to a large extent, resemble the structures exhibited by the general model of the complex Ginzburg-Landau equation with global feedback [15,27] where intermittent turbulence, amplitude clusters, and oscillatory cellular arrays were also found. Thus, we expect that many of the observed phenomena can be also found in other reaction-diffusion systems of various origins.

ACKNOWLEDGMENT

We gratefully acknowledge financial support of the Deutsche Forschungsgemeinschaft in the framework of Sonderforschungsbereich 555 ''Complex Nonlinear Processes.''

APPENDIX: TRANSFORMATION TO PHASE AND AMPLITUDE VARIABLES

Theoretical studies of pattern formation in oscillatory reaction-diffusion systems are often performed in the framework of the CGLE, which is the amplitude equation of a field

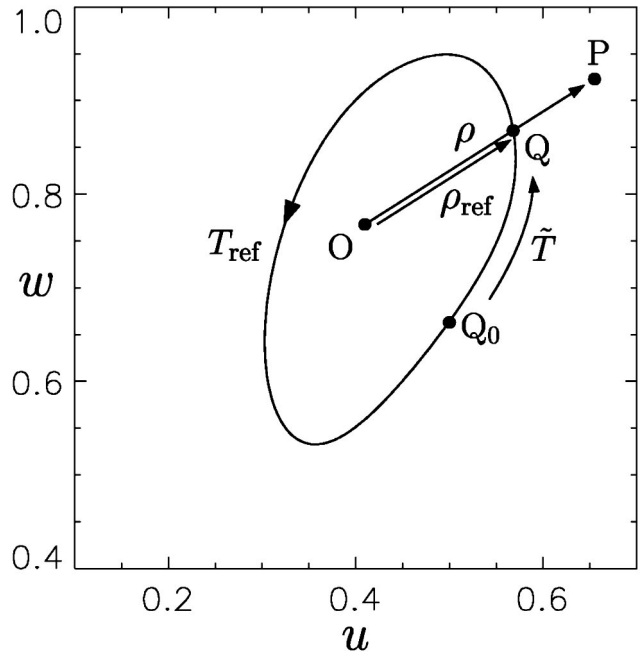

FIG. 14. Definition of the amplitude $R=\rho/\rho_{\mathrm{ref}}$ and phase $\phi=2\pi\tilde{T}/T_{\mathrm{ref}}$ for nonharmonic oscillations.

of diffusively coupled Hopf oscillators. Although this equation is strictly valid only close to the soft onset of oscillations, the results can often be successfully used to interpret experimental or numerical data, even in cases when oscillations have large amplitude and are nonharmonic. To provide a link to the general studies performed in the framework of the CGLE, it would thus be convenient to have amplitude and phase variables also defined for anharmonic oscillations, in such a way that they can be compared to the amplitude and the phase of harmonic oscillations in the normal form theory.

The variable transformation suggested in Ref. [19] was developed to realize this idea. It is an empirical method to transform a pair of model variables into an amplitude and a phase variable after computational modeling. Here, amplitude and phase are defined in the projection plane of the two model variables u and w. A reference trajectory for the dynamics defined in this plane is introduced to approximately compensate for deviations from harmonicity in the oscillations.

The transformation is illustrated in Fig. 14. Suppose that the reference trajectory is the closed orbit. The reference orbit can, for instance, be chosen as the long-time average of the projected local trajectories, or, as it was done here, be determined by an additional numerical simulation of model (1)–(3) in the absence of diffusion ($D=0$), where the control signal previously generated by the diffusive system was applied as p_{CO} forcing. Note that for periodic uniform oscillations, the reference trajectory exactly corresponds to the projection of the limit cycle.

An amplitude R and a phase ϕ for any local system state P with coordinates (u,w) in the projection plane can now be defined in the following way. First, the radius vector of

length $\rho=\overline{OP}$ and the point Q where this radius (or its extension) intersects with the reference orbit are determined. The amplitude for the point P is then defined as $R=\rho/\rho_{\mathrm{ref}}$, where the length $\rho_{\mathrm{ref}}=\overline{OQ}$ is used as a reference radius. For definition of the phase, some ''initial'' point Q_0 is marked on the orbit and the time $\tilde{T}$ needed to reach point Q along the reference cycle is determined. The phase is then defined as $\phi=2\pi\tilde{T}/T_{\mathrm{ref}}$, where T_{ref} is the period of the reference orbit.

Note that according to this definition, the amplitude is $R=1$ as long as the system stays on the reference orbit. Moreover, for the motion corresponding to the reference orbit, the phase ϕ increases at a constant velocity with time and changes by 2π after each period. When local oscillations are nearly harmonic and the reference orbit is a circle with point O in its center, the above definition yields the usual phase and amplitude variables. For further details on the transformation to amplitude and phase variables refer to Ref. [19].

[1] M.C. Cross and P.C. Hohenberg, Rev. Mod. Phys. **65**, 851 (1993).
[2] E. Benkler, M. Kreuzer, R. Neubecker, and T. Tschudi, Phys. Rev. Lett. **84**, 879 (2000).
[3] W. Wang, I.Z. Kiss, and J.L. Hudson, Phys. Rev. Lett. **86**, 4954 (2001).
[4] V.K. Vanag, L. Yang, M. Dolnik, A.M. Zhabotinsky, and I.R. Epstein, Nature (London) **406**, 389 (2000).
[5] M. Kim, M. Bertram, M. Pollmann, A. von Oertzen, A.S. Mikhailov, H.H. Rotermund, and G. Ertl, Science **292**, 1357 (2001).
[6] T. Sakurai, E. Mihaliuk, F. Chirila, and K. Showalter, Science **296**, 2009 (2002).
[7] V. Petrov, Q. Ouyang, and H.L. Swinney, Nature (London) **388**, 655 (1997).
[8] A.L. Lin, M. Bertram, K. Martinez, H.L. Swinney, A. Ardelea, and G.F. Carey, Phys. Rev. Lett. **84**, 4240 (2000).
[9] V.K. Vanag, A.M. Zhabotinsky, and I.R. Epstein, Phys. Rev. Lett. **86**, 552 (2001).
[10] A. Schrader, M. Braune, and H. Engel, Phys. Rev. E **52**, 98 (1995).
[11] I. Sendiña-Nadal, E. Mihaliuk, J. Wang, V. Pérez-Muñuzuri, and K. Showalter, Phys. Rev. Lett. **86**, 1646 (2001).
[12] I. Aranson, H. Levine, and L. Tsimring, Phys. Rev. Lett. **72**, 2561 (1994).
[13] M.E. Bleich and J.E.S. Socolar, Phys. Rev. E **54**, R17 (1996).
[14] R. Martin, A.J. Scroggie, G.-L. Oppo, and W.J. Firth, Phys. Rev. Lett. **77**, 4007 (1996).
[15] D. Battogtokh and A.S. Mikhailov, Physica D **90**, 84 (1996).
[16] S. Grill, V.S. Zykov, and S.C. Müller, Phys. Rev. Lett. **75**, 3368 (1995).
[17] V.S. Zykov, A.S. Mikhailov, and S.C. Müller, Phys. Rev. Lett. **78**, 3398 (1997).
[18] L. Yang, M. Dolnik, A.M. Zhabotinsky, and I.R. Epstein, Phys. Rev. E **62**, 6414 (2000).
[19] M. Bertram and A.S. Mikhailov, Phys. Rev. E **63**, 066102 (2001).
[20] M. Pollmann, M. Bertram, and H.H. Rotermund, Chem. Phys. Lett. **346**, 123 (2001).
[21] O.-U. Kheowan, C.-K. Chan, V.S. Zykov, O. Rangsiman, and S.C. Müller, Phys. Rev. E **64**, 035201(R) (2001).
[22] T. Pierre, G. Bonhomme, and A. Atipo, Phys. Rev. Lett. **76**, 2290 (1996).
[23] M. Münkel, F. Kaiser, and O. Hess, Phys. Rev. E **56**, 3868 (1997).
[24] G. Franceschini, S. Bose, and E. Schöll, Phys. Rev. E **60**, 5426 (1999).
[25] O. Beck, A. Amann, E. Schöll, J.E.S. Socolar, and W. Just, Phys. Rev. E **66**, 016213 (2002).
[26] M. Bertram, C. Beta, M. Pollmann, A. S. Mikhailov, H. H. Rotermund, and G. Ertl, Phys. Rev. E **67**, 036208 (2003).
[27] D. Battogtokh, A. Preusser, and A.S. Mikhailov, Physica D **106**, 327 (1997).
[28] R. Imbihl and G. Ertl, Chem. Rev. **95**, 697 (1995).
[29] T. Gritsch, D. Coulman, R.J. Behm, and G. Ertl, Phys. Rev. Lett. **63**, 1086 (1989).
[30] H.H. Rotermund, Surf. Sci. Rep. **29**, 265 (1997).
[31] K. Krischer, M. Eiswirth, and G. Ertl, J. Chem. Phys. **96**, 9161 (1992).
[32] A. von Oertzen, H.H. Rotermund, A.S. Mikhailov, and G. Ertl, J. Phys. Chem. B **104**, 3155 (2000).
[33] M. Bär, N. Gottschalk, M. Eiswirth, and G. Ertl, J. Chem. Phys. **100**, 1202 (1994).
[34] M. Bär and M. Eiswirth, Phys. Rev. E **48**, R1635 (1993).
[35] M. Hildebrand, M. Bär, and M. Eiswirth, Phys. Rev. Lett. **75**, 1503 (1995).
[36] M. Falcke and H. Engel, J. Chem. Phys. **101**, 6255 (1994).
[37] M. Falcke, H. Engel, and M. Neufeld, Phys. Rev. E **52**, 763 (1995).
[38] M. Falcke and H. Engel, Phys. Rev. E **56**, 635 (1997).
[39] M. Bertram and A. S. Mikhailov, Computer videos of two-dimensional spatiotemporal patterns in the model of CO oxidation under global delayed feedback, in: http://www.fhi-berlin.mpg. de/~complsys
[40] Y. Kuramoto, *Chemical Oscillations, Waves, and Turbulence* (Springer, Berlin, 1984).
[41] I.S. Aranson and L. Kramer, Rev. Mod. Phys. **74**, 99 (2002).
[42] A. S. Mikhailov and A. Y. Loskutov, *Foundations of Synergetics II* (Springer, Berlin, 1996).
[43] F. Mertens, R. Imbihl, and A. Mikhailov, J. Chem. Phys. **101**, 9903 (1994).
[44] H. Chaté, Nonlinearity **7**, 185 (1994).
[45] P. Coullet, J. Lega, B. Houchmanzadeh, and J. Lajzerowicz, Phys. Rev. Lett. **65**, 1352 (1990).
[46] D. Lima, D. Battogtokh, A. Mikhailov, P. Borckmans, and G. Dewel, Europhys. Lett. **42**, 631 (1998).